JTTEE5 17:942–947
DOI: 10.1007/s11666-008-9260-7
1059-9630/$19.00 © ASM International

Microstructure and Oxidation Behavior of Cr39Ni7C Cermet Coatings Deposited by Diamond Jet Spray Process

F.-X. Ye, S.-H. Wu, and A. Ohmori

(Submitted May 15, 2008; in revised form September 14, 2008)

For the promising erosion and oxidation resistance of carbide cermet coating, Cr39Ni7C cermet coatings were deposited by Diamond Jet spray process using a commercial Sulzer Metco 5241 powder in this study. The microstructure, phase compositions, and high-temperature oxidation behavior of the deposited coatings were investigated. The speed and temperature of in-flight particles were measured by DPV-2000. The results revealed that the speed of in-flight particles decreased from 229 to 150 m/s with the increasing of the spraying distance from 100 to 300 mm, whereas the average temperature of in-flight particles increased from 1926 to 2245 K. The decarburization of Cr_3C_2 increased with the increasing of the fuel gas flow from 58 SLPM to 77 SLPM for higher heat enthalpy of the flame. Due to the formation of Cr_2O_3 on/in the coatings at high temperature, the sprayed coatings had good oxidation resistance at 1073 K in an air atmosphere. The oxidation behavior was found to be governed by the parabolic rate law. For the lower porosity of the coating deposited under the spraying distance of 150 mm, its oxidation resistance was better than that of the coating sprayed at the spraying distance of 200 mm. A slight reduction of sprayed Cr39Ni7C cermet coating in micro hardness occurred after high temperature at 723 K and 1073 K high-temperature oxidation.

Keywords cermet coatings, HVOF microstructures, influence of properties

1. Introduction

Thermal spraying is an expanding area within the technology of surface engineering. It is a process that involves the deposition of molten or semi-molten droplets of powder on to a substrate to form a coating (Ref 1). Tungsten carbide and chromium carbide-based coatings are frequently used in various industrial fields such as the power generation industry and aerospace industry to improve the resistance to sliding, abrasive and erosive wear, and high-temperature oxidation (Ref 2-12). Although the wear resistance is lower compared with WC-Co cermet's, the Cr_3C_2-NiCr system exhibits a high oxidation resistance up to over 850 °C, while the WC-Co system will be severely oxidized at the temperature over 500 °C (Ref 13-16). Therefore, the Cr_3C_2-NiCr alloy cermet coatings have been widely used for high-temperature wear resistance and corrosion resistance applications. WC and Cr_3C_2 with different metallic binders like Co, Ni, and Fe have been studied using different amounts of binder contents with Co and Ni most commonly used. Addition of Cr to the matrix has been found to improve the wear and oxidation resistance of these cermets (Ref 17).

Oxygen and a fuel gas in high velocity oxy-fuel (HVOF) spraying flow at high pressures and flow-rates with internal combustion to produce very high particle velocities with relatively low temperatures compared with other thermal spray processes such as air or vacuum plasma spraying. As a result, HVOF is capable of producing dense coatings with low degrees of decomposition, which are well bonded to the substrate (Ref 1). It has been reported that carbide containing coatings deposited by high velocity processes have good wear resistance compared to plasma-sprayed coatings due to the better coating properties achievable using high velocity processes (Ref 17).

In this study, Cr39Ni7C powder that has much more NiCr compared with commonly applied Cr_3C_2-25NiCr powder was used as the feedstock powder for high-temperature applications up to 900 °C. The temperature and velocity of the in-flight particles were measured by DPV-2000, and the microstructure and high-temperature oxidation behavior of the coatings deposited by the Diamond Jet method were characterized and discussed.

This article is an invited paper selected from presentations at the 2008 International Thermal Spray Conference and has been expanded from the original presentation. It is simultaneously published in *Thermal Spray Crossing Borders, Proceedings of the 2008 International Thermal Spray Conference*, Maastricht, The Netherlands, June 2-4, 2008, Basil R. Marple, Margaret M. Hyland, Yuk-Chiu Lau, Chang-Jiu Li, Rogerio S. Lima, and Ghislain Montavon, Ed., ASM International, Materials Park, OH, 2008.

F.-X. Ye, School of Materials Science and Engineering, Tianjin University, Weijin Road No.92, Tianjin 300072, People's Republic of China; **S.-H. Wu**, Suzhou Nuclear Power Research Institute, Suzhou, People's Republic of China; and **A. Ohmori**, TOCALO Co. Ltd., Minamifutami, Futami-Cho, Akashi, Japan. Contact e-mail: yefx@tju.edu.cn.

2. Materials and Experimental Procedure

2.1 Feedstock Powders and Substrate

The feedstock powder was Cr39Ni7C (available from Sulzer Metco 5241 powder). This consisted of fine particles that are obtained by melting a material having a composition of Cr:Ni:C = 54:39:7 (% by mass) and rapidly solidifying the melt, with Cr and C forming chromium carbide and Ni and Cr forming a Ni-Cr alloy by melting and rapid solidification. Sulzer Metco 5241 has a structure in which crystallized chromium carbide particles are dispersed in a Ni-Cr alloy (Ref 18, 19). The X-ray diffraction pattern of Cr39Ni7C powder is shown in Fig. 1. The size distribution of the Cr39Ni7C powder was −53 + 15 μm and its morphology is given in Fig. 2, The substrate for coating preparation was mild steel (JIS SS400) and its thickness was 5.7 mm. Prior to the coating, the mild steel substrates were cleaned with acetone and grit blasted using Al_2O_3 sand with average size of 830 μm.

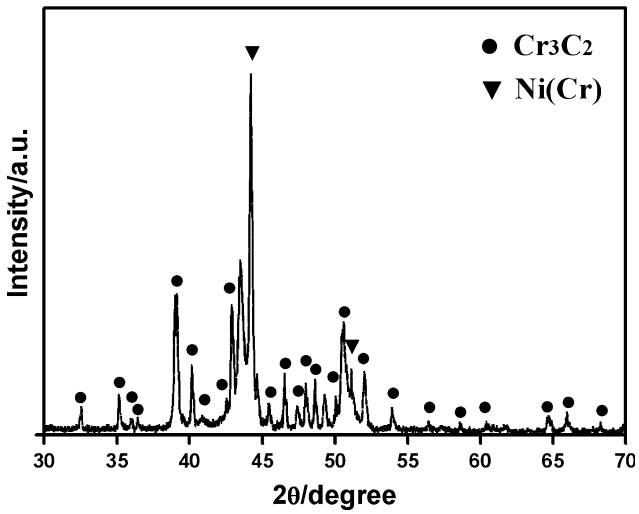

Fig. 1 X-ray diffraction pattern of the Cr39Ni7C feedstock powder

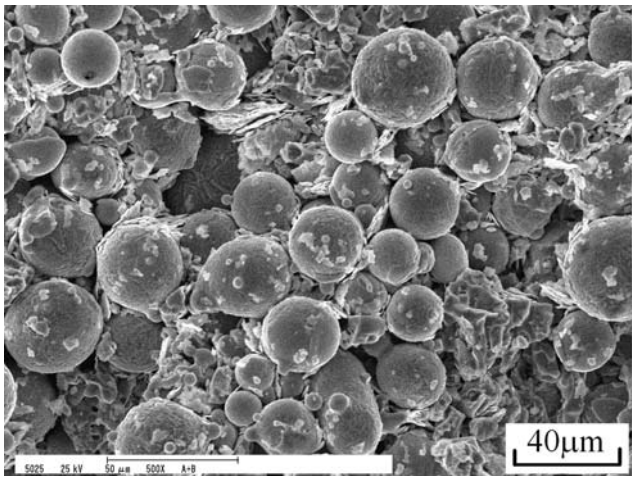

Fig. 2 Typical morphology of Cr39Ni7C feedstock powder

2.2 Thermal Spraying Equipment

The thermal spraying equipment was a commercial HVOF system (Diamond Jet 2600 manufactured by Sulzer Metco). The thermal spraying parameters are given in Table 1.

2.3 Temperature and Velocity of In-flight Particle

The temperature and velocity of the in-flight particles were measured by DPV-2000 equipment (Tecnar Automation Ltd., Canada). DPV-2000 applies infrared pyrometry along with a two-slit photo-mask in order to perform in-flight diagnostics on individual particles. A particle passing in front of the photo-mask will generate a two-peaks signal. The peaks distance and intensity are used to calculate the temperature and velocity of particle.

2.4 Analysis of Microstructure and Compositions

Scanning electron microscope (SEM) and energy dispersive X-ray analysis (EDAX) were used to examine the structure characteristics of the feedstock powder and the sprayed coatings. The phase compositions of the feedstock powder and the sprayed coatings were investigated by X-ray diffraction using Cu-Kα radiation (λ = 1.5406 Å) and a graphite crystal monochromator (JDX3530, JEOL, Japan). Vickers hardness of the sprayed coatings was measured using an automatic hardness testing machine (AAV-500, Akashi Group, Japan) with a 100 gf load for 15 s. An average hardness was calculated from five indents per specimen. The porosity of the coating was calculated using image software according to the coating's cross section of SEM image.

2.5 High-Temperature Oxidation of the Sprayed Coatings

Isothermal oxidation behavior of the sprayed coating was conducted at 1073 K up to 100 h in a programmable furnace. The coated sample size was 15 × 15 × 6.0 mm for oxidation experiment. The mass gain was measured by an analytical balance with a sensitivity of 0.1 mg.

Table 1 Diamond Jet 2600 spraying parameters

Propylene fuel gas pressure, MPa	0.69
Propylene fuel gas flow, SLPM	58, 67, 77
Oxygen gas pressure, MPa	1.03
Oxygen gas flow, SLPM	316
Air gas pressure, MPa	0.52
Air gas flow, SLPM	207
Argon carrier gas pressure, MPa	0.86
Argon carrier gas flow, SLPM	14
Spraying distance, mm	100-300

3. Results and Discussion

3.1 Temperature and Velocity of the In-flight Particles

Although HVOF processes minimize decomposition of the carbide phase due to lower heat enthalpy and shorter duration involved in the coating processes, the highest temperature of the in-flight particle is also a main factor to evaluate the decarburization of Cr_3C_2 in the thermal spraying of Cr_3C_2-NiCr materials. In addition, higher in-flight particle velocity during deposition provides several advantages such as lower porosity, higher bond strength and hardness. The temperature of the in-flight particle increased with the increasing of spraying distance from 150 to 300 mm, while the velocity decreased from 230 to 150 m/s (Fig. 3). It is reported that the decomposition temperature of Cr_3C_2 is 2168 K (Ref 20, 21). The average temperature of the in-flight particle did not exceed 2168 K with spraying distance shorter than 250 mm.

3.2 Microstructure and Compositions of As-Sprayed Coatings

Figure 4 shows the cross sectional microstructure of Cr39Ni7C coating sprayed with the fuel gas flow of 67 SLPM and spraying distance of 225 mm. According to Fig. 4a, the Cr_3C_2 particles were much finer than that in the general thermal-sprayed Cr_3C_2-25%NiCr coating with average particle size of 2-4 micrometers (Ref 13, 17). The as-sprayed coating had a dense structure with a homogenous distribution of fine-grained carbide. Using SEM-EDAX and XRD analysis, the dark area was composed of a finely dispersed chromium carbide phase (dark) surrounded by layers of metal matrix (lighter). Generally, the spraying distance has been observed to have a great influence on the coating porosity. This conclusion was also observed in this study. With the increasing of spraying distance from 150 to 200 mm, the porosity of the coating increased from 0.4 to 4.6% at the fuel gas flow of 77 SLPM.

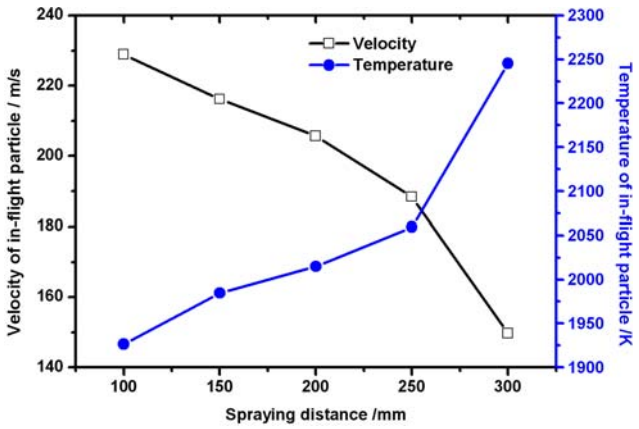

Fig. 3 The dependence of temperature and velocity of in-flight Cr39Ni7C particles with the spraying distance in Diamond Jet spraying

The X-ray diffraction patterns of the Diamond Jet-sprayed Cr39Ni7C coatings under the different fuel gas flow are illustrated in Fig 5. Dissolution of carbide into the matrix and the consequent super saturation of the matrix with Cr and C gave rise to a large amorphous background on the low angle side of the NiCr peak in the XRD scan. The only detectable crystalline phases were Cr_3C_2, NiCr, and Cr_2O_3. While small amounts of Cr_7C_3 may have formed through decarburization of Cr_3C_2, its concentration was too low to be distinguished from other overlapping peaks. A small amount of Cr_2O_3 was formed during thermal spraying. With the increasing of fuel gas flow from 58 SLPM to 77 SLPM, the intensity of Cr_3C_2 peak decreased for the higher heat enthalpy of flame. The Cr_3C_2 decomposed more with higher fuel gas flow in the thermal spraying processes.

3.3 Isothermal Oxidation Behavior of Sprayed Coatings

In all cases, a black tarnish layer had formed on the coatings surface after high-temperature oxidation exposure. The X-ray diffraction pattern of the sprayed coating

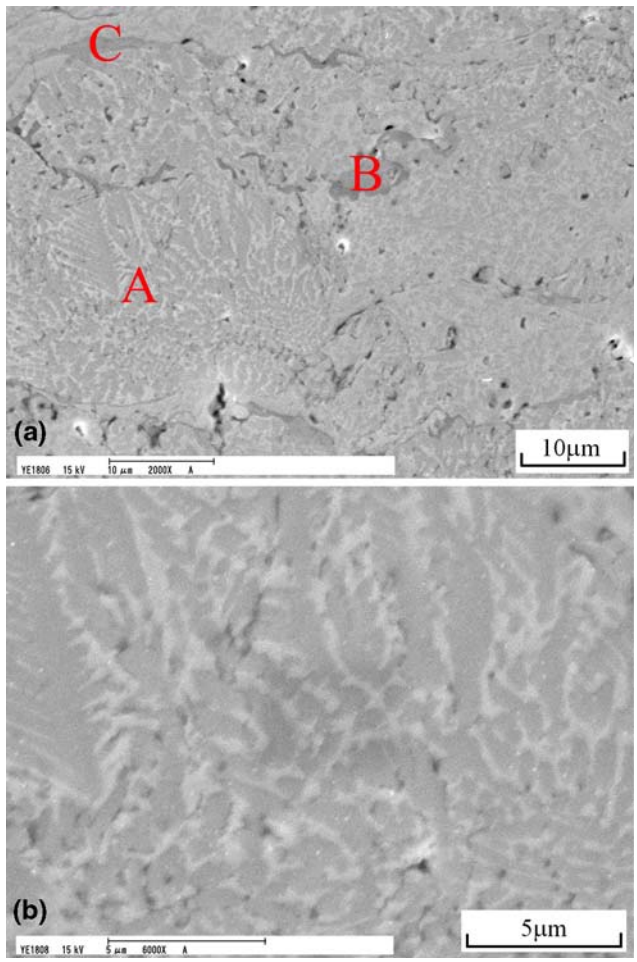

Fig. 4 The cross sectional microstructure of Cr39Ni7C coating sprayed under the fuel gas flow of 67 SLPM and spraying distance of 225 mm. ((a) low magnification, (b) high magnification of area "A" in (a), Note: gray "B" and "C" were Cr_3C_2)

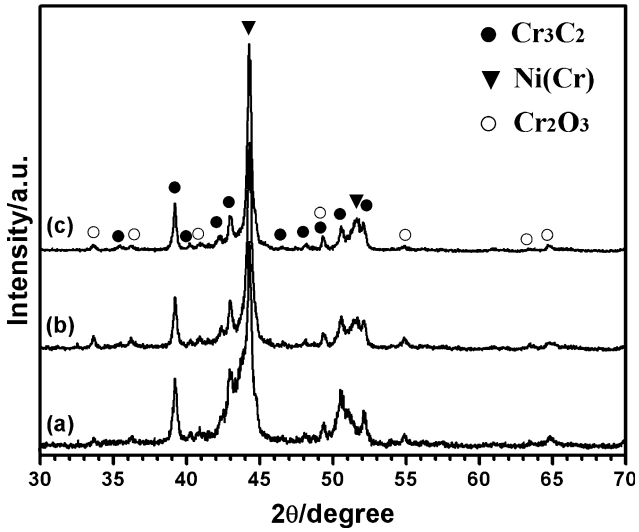

Fig. 5 The X-ray diffraction patterns of Cr39Ni7C coatings sprayed under different fuel gas flow and spraying distance of 225 mm ((a) Fuel gas flow 58 SLPM, (b) Fuel gas flow 67 SLPM, (c) Fuel gas flow 77 SLPM)

after the high-temperature experiment is shown in Fig. 6. It indicated that the patterns of the coatings after oxidation were dominated by narrow crystalline peaks of Cr_3C_2, NiCr, and Cr_2O_3. A large amount of Cr_2O_3 was formed on the coating after 100 h of high-temperature oxidation at 1073 K due to the reaction of Cr with oxygen in air. As a result, the components of the coating structure were changed and the coating was covered by formed Cr_2O_3. Therefore, the corrosion progress of the coating was retarded.

The squares of the mass gain as a function of oxidation time for the coated and bare SS400 at 1073 K are shown in Fig. 7. The weight gains of the coated SS400 are much less than that of the bare SS400 during the oxidation experiments. The roughly straight-line relationship indicates that the oxidation kinetic of the bare and coated SS400 samples was governed by parabolic rate law $y^2 = kt$. The parabolic rate constants (k) for bare SS400, the coated SS400 by Cr39Ni7C coatings prepared with spraying distance of 200 mm and 150 mm were 1.3×10^{-6} $mg^2mm^{-4}s^{-1}$, 3.4×10^{-7} $mg^2mm^{-4}s^{-1}$, 2.5×10^{-7} $mg^2mm^{-4}s^{-1}$, respectively. It is apparent that for the Cr39Ni7C coated SS400, the parabolic rate constants for oxidation decreased by about one order of magnitude at temperature of 1073 K. The oxidation resistance of Cr39Ni7C coating sprayed at the spraying distance of 150 mm was better than that of the sprayed at 200 mm. This was attributed partially to its lower porosity as discussed in section 3.2.

3.4 Microhardness Variation of Cr39Ni7C Coatings

The complex metastable state of the as-sprayed coating means that there is a large driving force for microstructural and compositional transformations when exposed to elevated temperatures. The most notable change is the precipitation of fine carbides or possibly oxides accompanied by recrystalization of the matrix. The mechanical

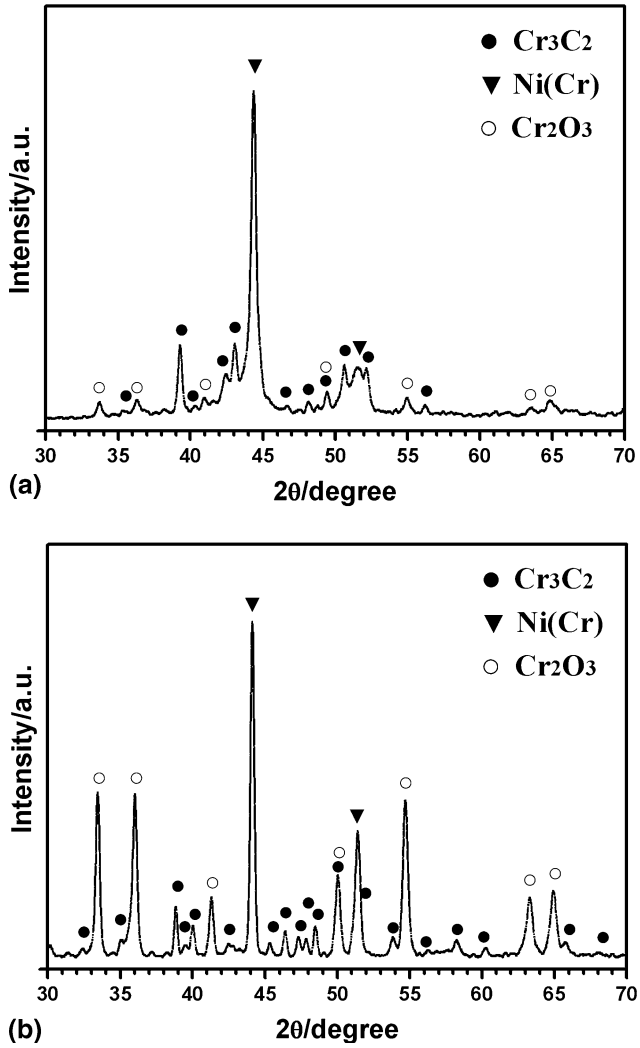

Fig. 6 The X-ray diffraction patterns of as sprayed (a) and 1073 K during 100 h heat treated (b) Cr39Ni7C coatings (Fuel gas flow: 77 SLPM, Spraying distance: 150 mm)

properties also change, in particular the microhardness, which is commonly related to the performance of carbide coatings under wear conditions (Ref 22). The Vickers hardness of the sprayed coatings after high-temperature oxidation is given in Fig. 8. The average Vickers hardness of the coatings sprayed under a fuel gas flow of 77 SLPM and spraying distance of 150 mm was approximated to 1126 $HV_{0.1}$. A slight reduction in micro hardness occurred after 115 h at 723 K high-temperature oxidation and after 100 h at 1073 K high-temperature oxidation. This may result from the residual stress relief, carbide dissolution, and matrix phase refinement, which were also reported by S. Matthews (Ref 22).

4. Conclusions

The microstructure, phase compositions, and high-temperature oxidation behavior of the deposited cermet

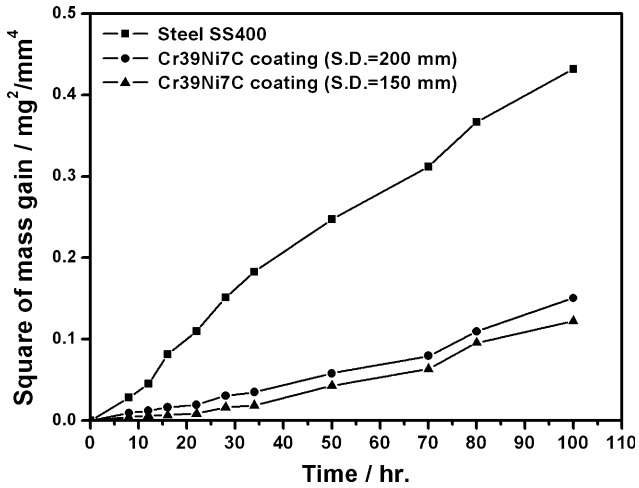

Fig. 7 Squares of the mass gain as a function of oxidation time at 1073 K for bare SS400 and Cr39Ni7C coating sprayed at the spraying distance (S.D.) of 150 mm and 200 mm

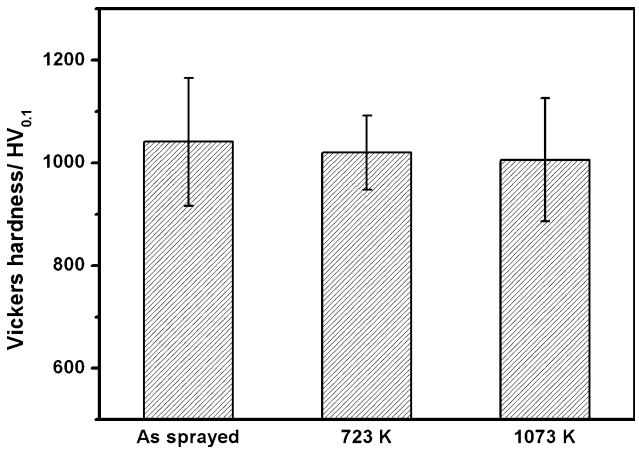

Fig. 8 Vickers hardness of the Cr39Ni7C-sprayed coatings after 115 h at 723 K and 100 h at 1073 K high-temperature oxidation

Cr39Ni7C coatings were investigated. The speed of in-flight particles decreased from 229 to 150 m/s with the increasing of spraying distance from 100 to 300 mm, whereas the average temperature of in-flight particles increased from 1926 to 2245 K. The decarburization of Cr_3C_2 increased with the increasing of fuel gas flow from 58 SLPM to 77 SLPM for higher heat enthalpy of flame. Due to the formation of Cr_2O_3 on/in the coatings at high temperature, the sprayed coatings had good oxidation resistance at 1073 K in air atmosphere. The oxidation behavior was found to be governed by the parabolic rate law. For the lower porosity of the coating deposited under the spraying distance of 150 mm, its oxidation resistance was better than that sprayed under the spraying distance of 200 mm. The average Vickers hardness of the coatings sprayed under fuel gas flow of 77 SLPM and spraying distance of 150 mm was approximated to 1126 $HV_{0.1}$. A slight reduction of sprayed Cr39Ni7C cermet coating in micro hardness occurred after 115 h in 723 K high-temperature oxidation and after 100 h in 1073 K high-temperature oxidation.

Acknowledgments

This work was partly supported by the Tianjin Natural Scientific Research Foundation (No. 07JCYBJC18200), and by the Research Fund for the Doctoral Program of Higher Education of China (No. 20070056097) and by the National Natural Science Foundation of China (No. 50805104).

References

1. S. Wirojanupatump, P.H. Shipway, and D.G. McCartney, The Influence of HVOF Powder Feedstock Characteristics on the Abrasive Wear Behaviour of Cr_xC_y-NiCr Coatings, *Wear*, 2001, **249**, p 829-837
2. M.H. Staia, T. Valente, C. Bartuli, D.B. Lewis, and C.P. Constable, Part I: Characterization of Cr_3C_2-25%NiCr Reactive Plasma Sprayed Coatings Produced at Different Pressures, *Surf. Coat. Technol.*, 2001, **146-147**, p 553-562
3. M.H. Staia, T. Valente, C. Bartuli, D.B. Lewis, C.P. Constable, A. Romand, J. Lesage, D. Chicot, and G. Mesmacque, Part II: Tribological Performance of Cr_3C_2-25%NiCr Reactive Plasma Sprayed Coatings Deposited at Different Pressures, *Surf. Coat. Technol.*, 2001, **146-147**, p 563-570
4. M. Mohanty, R.W. Smith, M. De Bonte, L.P. Celis, and E. Lugscheider, Sliding Wear Behaviour of Thermally Sprayed 75/25 Cr_3C_2/NiCr Wear Resistant Coatings, *Wear*, 1996, **198**, p 251-266
5. G.Z. Xie, Y.J. Lu, Z.Y. He, B. Hu, K.Y Wang, X.Y Mo, Y.P. Wu, and P.H Lin, Microstructure and Corrosion Properties of Plasma-Sprayed NiCr-Cr_3C_2 Coatings Comparison with Different Post Treatment, *Surf. Coat. Technol.*, 2008, **202**, p 2885-2890
6. K.J. Stein, B.S. Schorr, and A.R. Marder, Erosion of Thermal Spray MCr-CrC Cermet Coatings, *Wear*, 1999, **224**, p 153-159
7. B.Q. Wang and A. Verstak, Elevated Temperature Erosion of HVOF Cr_3C_2/TiC-NiCrMo Cermet Coating, *Wear*, 1999, **233-235**, p 342-351
8. J. Wang, L. Zhang, B.D. Sun, and Y.H Zhou, Study of the Cr_3C_2-NiCr Detonation Spray Coating, *Surf. Coat. Technol.*, 2000, **130**, p 69-73
9. Y. Ishikawa, S. Kuroda, J. Kawakita, Y. Sakamoto, and M. Takaya, Sliding Wear Properties of HVOF Sprayed WC-20%Cr_3C_2-7%Ni Cermet Coatings, *Surf. Coat. Technol.*, 2007, **201**, p 4718-4727
10. D. Toma, W. Brandl, and G. Marginean, Wear and Corrosion Behaviour of Thermally Sprayed Cermet Coatings, *Surf. Coat. Technol.*, 2001, **138**, p 149-158
11. X.M. Li, Y.Y. Yang, T.M. Shao, Y.S. Jin, and G. Barbezat, Impact Wear Performance of Cr_3C_2-NiCr Coatings by Plasma and HVOF Spraying, *Wear*, 1997, **202**, p 208-214
12. N. Espallargas, J. Berget, J.M. Guilemany, A.V. Benedetti, and P.H. Suegama, Cr_3C_2-NiCr and WC-Ni Thermal Spray Coatings as Alternatives to Hard Chromium for Erosion-Corrosion Resistance, *Surf. Coat. Technol.*, 2008, **202**, p 1405-1417
13. G.C. Ji, C.J. Li, Y.Y. Wang, and W.Y. Li, Microstructural Characterization and Abrasive Wear Performance of HVOF Sprayed Cr_3C_2-NiCr Coating, *Surf. Coat. Technol.*, 2006, **200**, p 6749-6757
14. C.J. Li, Y.Y. Wang, T. Wu, G.C. Ji, and A. Ohmori, Effect of Types of Ceramic Materials in Aggregated Powder on the Adhesive Strength of High Velocity Oxy-Fuel Sprayed Cermet Coatings, *Surf. Coat. Technol.*, 2001, **145**, p 113-120
15. C.J. Li, G.C. Ji, Y.Y. Wang, and K. Sonoya, Dominant Effect of Carbide Rebounding on the Carbon Loss During High Velocity Oxy-Fuel Spraying of Cr_3C_2-NiCr, *Thin Solid Films*, 2002, **419**, p 137-143

16. T.S. Sidhu, S. Prakash, and R.D. Agrawal, Hot Corrosion Studies of HVOF Sprayed Cr_3C_2-NiCr and Ni-20Cr Coatings on Nickel-Based Superalloy at 900°C, *Surf. Coat. Technol.*, 2006, **201**, p 792-800
17. J.K.N. Murthy and B. Venkataraman, Abrasive Wear Behaviour of WC-CoCr and Cr_3C_2-20(NiCr) Deposited by HVOF and Detonation Spray Processes, *Surf. Coat. Technol.*, 2006, **200**, p 2642-2652
18. http://www.freepatentsonline.com/20060040125.html, ''Piston Ring and Thermal Spray Coating Used Therein, and Method for Manufacturing Thereof,'' United States Patent 20060040125. Accessed 10 May 2007
19. http://www.sulzermetco.com/en/Portaldata/13/Resources/2_Products_Services/Thermal_Spray_Materials_Guide_022006.pdf, *Sulzer Metco Thermal Spray Materials Guide*, Issued April 2005, p HVOF-13. Accessed 10 May 2007
20. E. Yun and S. Lee, Correlation of Microstructure with Hardness and Wear Resistance in Cr_3C_2/Stainless Steel Surface Composites Fabricated by High-Energy Electron Beam Irradiation, *Mater. Sci. Eng., A*, 2005, **405**, p 163-172
21. K. Hirota, K. Mitani, M. Yoshinaka, and O. Yamaguchi, Simultaneous Synthesis and Consolidation of Chromium Carbides (Cr_3C_2, Cr_7C_3 and $Cr_{23}C_6$) by Pulsed Electric-Current Pressure Sintering, *Mater. Sci. Eng., A*, 2005, **399**, p 154-160
22. S. Matthews, M. Hyland, and B. James, Microhardness Variation in Relation to Carbide Development in Heat Treated Cr_3C_2-NiCr Thermal Spray Coatings, *Acta Mater.*, 2003, **51**, p 4267-4277